Int. J. Heat Mass Transfer. Vol. 22, pp. 669–678
© Pergamon Press Ltd. 1979. Printed in Great Britain

0017 9310/79/0501-0669 $02.00/0

POST DRYOUT HEAT TRANSFER TO R-113 UPWARD FLOW IN A VERTICAL TUBE

YASUO KOIZUMI,† TATSUHIRO UEDA and HIROAKI TANAKA
Department of Mechanical Engineering, University of Tokyo, Bunkyo-ku, Tokyo, Japan

(*Received* 22 *July* 1978)

Abstract—An analysis of heat transfer in the post dryout region of upflow in a uniformly heated tube was performed on the basis of the three path heat-transfer model, involving heat-transfer processes from wall to vapor, from vapor to liquid droplets and from wall to droplets in contact with the wall. Wall temperature distribution was predicted by solving a set of equations describing the variations of droplet diameter, actual quality, vapor temperature and droplet velocity along the tube downstream of the dryout point. The predicted wall temperature distributions show a good agreement with the experimental data for R-113 presented in the previous report. This result indicates that most of the heat from the heating wall is transferred to the vapor flow and droplets vaporize principally in the superheated vapor flow.

NOMENCLATURE

B, non-dimensional Spalding transport number;
C, droplet concentration [kg/m^3];
C_D, drag coefficient of evaporating droplet;
C_{DO}, drag coefficient of solid sphere;
c_p, specific heat [J/kg];
D, tube diameter [m];
d, droplet diameter [m];
$\bar{d}_1$, arithmetical mean diameter [m];
$\bar{d}_2$, $\bar{d}_3$, $\bar{d}_4$, characteristic droplet diameters [m];
g, acceleration of gravity [m/s^2];
h_{fg}, heat of vaporization [J/kg], [kJ/kg];
K, droplet transfer coefficient [m/s];
$\dot{M}$, mass flowrate [kg/s], [kg/h];
$\dot{m}_D$, droplet mass transfer rate per unit area [kg/(m^2 s)];
N, density of droplets [droplets/m^3];
Pr, prandtl number;
p, pressure [N/m^2], [bar];
$\dot{q}_{g\delta}$, heat-transfer rate from vapor to droplets per unit wall surface [W/m^2];
$\dot{q}^*_{g\delta}$, heat-transfer rate from vapor to droplets per unit droplet surface [W/m^2];
$\dot{q}_w$, heat flux from the wall [W/m^2];
$\dot{q}_{wg}$, heat-transfer rate from wall to vapor [W/m^2];
$\dot{q}_{w\delta}$, heat-transfer rate from wall to droplets [W/m^2];
Re, Reynolds number;
T, temperature [°C];
t, time [s];
u, velocity [m/s];
We, Weber number;
x, quality;
x_A, actual quality;
x_E, equilibrium quality;
y, distance from dryout point [m];
z, distance from the beginning of heating section [m].

Greek symbols

α, heat-transfer coefficient [W/(m^2 °C)];
$\gamma(B)$, shielding function;
ε, heat-transfer effectiveness;
λ, thermal conductivity [W/(m °C)];
ν, kinematic viscosity [m^2/s];
ρ, density [kg/m^3];
σ, surface tension [N/m].

Subscripts

b, bulk;
DP, dryout point;
f, film temperature of tube wall;
f^*, film temperature of droplet;
g, vapor;
in, inlet of tube;
l, liquid;
s, saturation;
T, total;
w, wall;
wi, inner wall;
δ, droplet;
δ^*, value evaluated per unit droplet surface.

1. INTRODUCTION

HEAT transfer to high quality two-phase flow in a heated channel has come of importance in recent years due to advancements in various technologies such as once-through steam generators and nuclear reactors.

In a previous paper [1] the authors presented a heat-transfer experiment on high quality upward flow in a uniformly heated tube, made with a fluorinated chloroethane R-113 at 3 bar as the test fluid. In the paper attention was focused on the process leading to dryout of the liquid film on the

†Present address: Japan Atomic Energy Research Institute, Tokai-mura, Ibaraki, Japan.

heated wall. Then, the droplet transfer rate onto the wall surface as well as the initial flowrate of the liquid film were measured at the inlet of the test tube by attaching equipment designed for the purpose. From these data, the variation of the liquid film flowrate along the tube was analyzed. The results showed that the characteristic sharp rise in wall temperature originated at the position where the calculated liquid film flowrate became nearly equal to zero. This present paper is concerned with another phase of the authors' experiment and interest is directed to the heat-transfer process in the post dryout regions.

A number of papers have been published on the post dryout heat transfer. Swenson *et al.* [2] and Polomik *et al.* [3] performed heat-transfer measurements for steam–water mixtures in order to provide design information for once-through power boilers and reactors. They correlated their data with modified forms of the generally accepted heat-transfer equations for single phase flow. A series of studies by Rohsenow *et al.* [4–9] dealt with dispersed flow film boiling. Their experimental works have been conducted mostly with nitrogen. They first attempted to analyze the dispersed flow boiling in terms of physical mechanisms involved. It has been assumed that heat transfer takes place in steps: from the wall to the vapor and then from the vapor to the droplets suspended in the stream; and from the wall to the droplets in contact with the wall. Convincing theoretical evidence was presented that there exists a significant thermodynamic non-equilibrium between the vapor and liquid droplets. Bennett *et al.* [10] and Keeys *et al.* [11] performed heat-transfer experiments of steam–water mixtures, and developed independently a similar analytical model which took into account the cooling of the superheated vapor by entrained liquid droplet evaporation, in disregard of direct cooling of the wall by impinging droplets.

The thermodynamic non-equilibrium causes considerably lower heat-transfer coefficients than are expected on the basis of thermodynamic equilibrium. The degree of thermodynamic non-equilibrium is considered to be determined by the rate of droplet evaporation in the superheated vapor stream. Thus heat transfer between vapor and droplets has to be closely examined. In this respect, estimation of droplet size becomes important. Rohsenow *et al.* [5] have suggested a value of 7.5 for an initial Weber number of droplets at the dryout point as well as for a critical Weber number for droplet breakup in the dispersed flow. On the other hand, Bennett *et al.* [10] and Keeys *et al.* [11] have chosen a constant value of 0.3 mm for an initial value of entrained droplet diameter. As for the heat-transfer coefficient between vapor and droplets, both Rohsenow and Bennett employed the equations for a solid sphere. However, vapor efflux from a droplet surface is expected to suppress heat transfer to the droplet.

In the present paper, a set of differential equations describing the heat-transfer processes in the post dryout region is numerically solved for typical runs of the authors' experiment, by introducing such values as initial droplet diameters and the droplet transfer coefficient determined experimentally. The calculated wall temperatures and vapor temperatures are compared with the measured wall temperature profiles and with the vapor temperatures measured at the exit of the tube. From the comparison and other predicted results, discussions of the mechanisms involved in the heat-transfer process are presented.

2. EXPERIMENTS

The heat-transfer experiment presented in the previous paper is outlined here. Further details of the apparatus and procedure are given in [1].

A schematic diagram of the test loop is shown in Fig. 1. The vapor–liquid mixture of R-113 flowed up in the lower tube (5) of 10 mm I.D. and 1.2 m long forming annular-dispersed two-phase flow. The liquid film on the tube wall was removed at a liquid film separator (6), and the remaining mist flow passed through the test tube (7) to a condenser (9).

The test tube placed vertically is made of a stainless-steel tube with well polished inner surface of 10.0 mm I.D., 12 mm O.D. and 2064 mm long. An intermediate section of 1461 mm in length was heated uniformly by passing an alternating current through the tube wall, whereas the preceding 253 mm and succeeding 350 mm sections were unheated.

A suction thermometer was mounted at the exit of the test tube for measuring the superheated vapor temperature in the mist flow. A suction tube of 5 mm

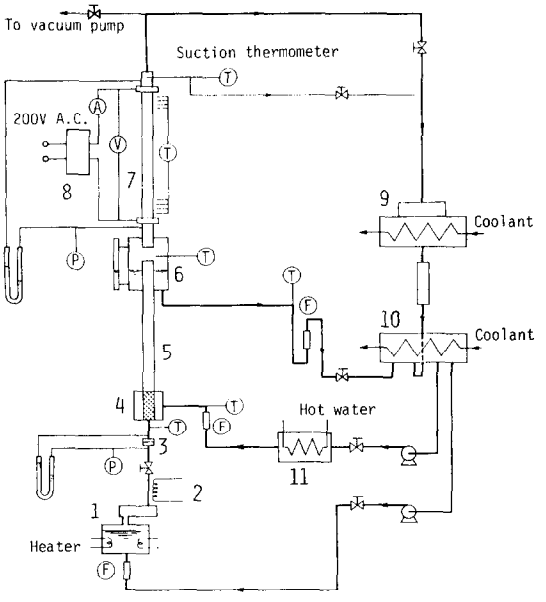

FIG. 1. Schematic diagram of experimental apparatus.

O.D. and 4 mm I.D. was inserted horizontally into the main stream. A thermocouple of 1.6 mm O.D. was installed in it to be sheltered from impinging droplets. A moderate suction through the tube permitted measurements of the superheated vapor temperature without the effect of entrained droplets.

The pressure p_{in} at the inlet of the test tube was adjusted to 3.05 bars. At this pressure, the saturation temperature of R-113 is 84.8°C, the heat of vaporization is 133 kJ/kg, and the densities of the saturated vapor and liquid are 20.8 kg/m^3 and 1410 kg/m^3, respectively. Heat transfer measurement was performed in the following ranges of the total flowrate $\dot{M}_T$, the inlet quality x_{in} and the wall heat flux $\dot{q}_w$.

$$\dot{M}_T = 90\text{–}260\,\text{kg/h},\quad x_{in} = 0.45\text{–}0.80,$$
$$\dot{q}_w \leqq 9.3 \times 10^4\,\text{W/m}^2.$$

3. ANALYSIS OF POST DRYOUT HEAT TRANSFER

The heat transfer in the post dryout region is assumed to consist of three heat-transfer paths:

(1) from wall to vapor flow: $\dot{q}_{wg}$,
(2) from wall to droplets in contact with the wall: $\dot{q}_{w\delta}$,
(3) from vapor to droplets suspended in the stream: $\dot{q}_{g\delta}$.

Since the wall temperature does not exceed 200°C by too much in the experiment mentioned previously, radiation has little effect on the heat transfer. Here, heat-transfer rates $\dot{q}_{wg}$, $\dot{q}_{w\delta}$ and $\dot{q}_{g\delta}$ are expressed on the basis of the unit surface area of the tube wall. The heat flux from the tube wall $\dot{q}_w$ is expressed as

$$\dot{q}_w = \dot{q}_{wg} + \dot{q}_{w\delta}. \tag{1}$$

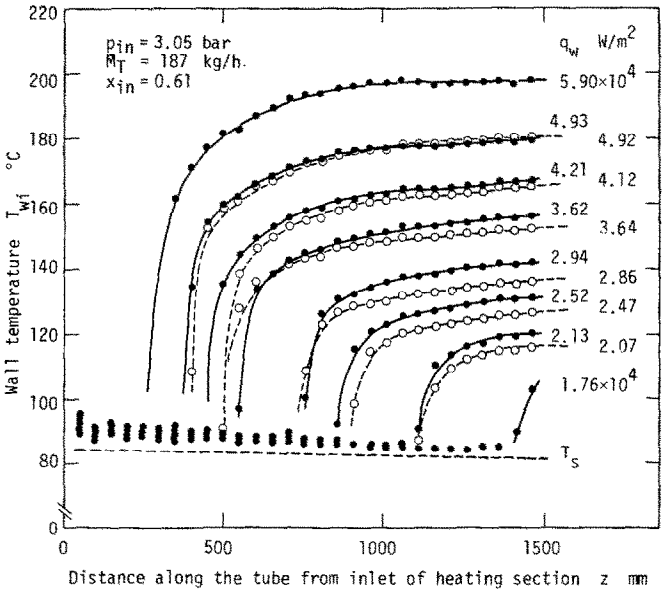

FIG. 2. Measured wall temperature profiles.

Figure 2 shows the typical experimental results of the inner wall temperature T_{wi} plotted against the distance z along the tube from the beginning of the heating section. The solid and open symbols in Fig. 2 represent the results obtained in the ways of increasing and decreasing the heat flux, respectively. A broken line in Fig. 2 denotes the saturation temperature T_s. The wall temperature is kept at low values slightly over the saturation temperature in the upper stream part of the test section, but it rises sharply at a particular point.

In this experiment, a thin liquid film was reformed on the wall surface in the preceding unheated section by deposition of droplets from the vapor stream. It was concluded in the previous paper [1] that the characteristic sharp rise in wall temperature originates at the position where the liquid flow-rate becomes nearly equal to zero. Thus, we may refer to this characteristic point as a dryout point.

The total heat-transfer rate to droplets per unit wall surface, $\dot{q}_\delta$, becomes

$$\dot{q}_\delta = \dot{q}_{w\delta} + \dot{q}_{g\delta}. \tag{2}$$

Various characteristic diameters of droplets are introduced in the analytical model mentioned below. From [1], the droplet size distribution at the inlet of the test tube is approximated by a gamma distribution, and characteristic diameters defined by $\bar{d}_2 = (\Sigma d^2/N_0)^{1/2}$, $\bar{d}_3 = (\Sigma d^3/\Sigma d)^{1/2}$ and $\bar{d}_4 = (\Sigma d^3/N_0)^{1/3}$ are expressed in terms of the arithmetical mean diameter $\bar{d}_1 = \Sigma d/N_0$ as follows:

$$\bar{d}_2 = 1.07\bar{d}_1,\ \bar{d}_3 = 1.23\bar{d}_1,\ \bar{d}_4 = 1.15\bar{d}_1, \tag{3}$$

where N_0 is the total number of droplets. $\bar{d}_2$ is concerned with the evaporation of droplets as well as the drag force acting on droplets, $\bar{d}_3$ is used to characterize droplet transfer onto the wall, and $\bar{d}_4$ represents the volume of droplets. Though the law of

droplet size distributions was determined from measurements at the inlet of the test tube [1], it is assumed in the following analysis that the correlations (3) hold at every station along the test tube.

3.1. *Heat-transfer rates* $\dot{q}_{wg}$, $\dot{q}_{w\delta}$ *and* $\dot{q}_{g\delta}$ *and wall temperature* T_{wi}

Dittus–Boelter correlation (4) has been verified in the authors' preliminary experiment of single phase heat transfer to superheated vapor of R-113:

$$\alpha_g = 0.023 \frac{\lambda_{gf}}{D} Re_{gf}^{0.8} Pr_{gf}^{0.4}. \tag{4}$$

This equation is then applicable to estimate the heat-transfer contribution of vapor flow in the post dryout region. In this case, $Re_{gf} = u_g D/v_{gf}$ and $u_g = M_T x_A/(\pi D^2 \rho_{gb}/4)$. When the thermodynamic non-equilibrium exists between the vapor and liquid, the actual quality $x_A = \dot{M}_g/\dot{M}_T$ is different from the equilibrium quality x_E defined by the following equation:

$$x_E = x_{in} + \frac{\pi D \dot{q}_w}{\dot{M}_T h_{fg}} z. \tag{5}$$

In the experimental system mentioned previously, the velocity profile of vapor flow at the dryout point is considered to be in a developed condition, whereas the thermal boundary layer of vapor flow starts afresh from the dryout point, where the vapor temperature is uniformly kept at the saturation temperature. Depew [12] has examined heat transfer to turbulent air flow in a uniformly heated tube with a fully developed velocity profile at the inlet. His experimental results are approximated as follows:

$$\frac{\alpha_{wg}(y/D)}{\alpha_{wg\infty}} = 1 + \frac{1.25}{(y/D)^{1.34}}, \tag{6}$$

where $\alpha_{wg}(y/D)$ is the heat-transfer coefficient at the distance y from the beginning of the heating section and $\alpha_{wg\infty}$ is that at a long distance downstream. Then, taking y for the distance from the dryout point, the heat-transfer coefficient of vapor flow in the post dryout region can be estimated from equation (4) with the aid of equation (6) as

$$\alpha_{wg} = 0.023 \frac{\lambda_{gf}}{D} Re_{gf}^{0.8} Pr_{gf}^{0.4} \left[1 + \frac{1.25}{(y/D)^{1.34}} \right]. \tag{7}$$

The heat-transfer rate $\dot{q}_{wg}$ from wall to vapor flow is obtained by

$$\dot{q}_{wg} = \alpha_{wg}(T_{wi} - T_g), \tag{8}$$

where T_g is the vapor temperature.

As for the heat-transfer rate $\dot{q}_{w\delta}$, Ueda *et al.* [13] have examined heat transfer to droplets impinging on a vertical hot surface. Here, we may define the heat-transfer effectiveness of individual droplets, ε, as the proportion of the heat removed by the impinging droplet to the heat required to vaporize the droplet entirely. Reference [13] shows that when the surface temperature is high and the impinging droplets cannot wet the surface, the heat-transfer effectiveness ε is considerably low ranging between 2–6%. In the following analysis we assume that ε is constant in the post dryout region regardless of the wall temperature variation. Then, droplets transferred onto the wall remove the following amount of heat:

$$\dot{q}_{w\delta} = \varepsilon \dot{m}_D h_{fg} \tag{9}$$

where $\dot{m}_D = KC$ is the droplet mass-transfer rate per unit surface area of the wall. K is the droplet transfer coefficient which is determined for the present experimental conditions from the empirical equation (14) of [1], and C is the mean concentration of droplets in mist flow:

$$C = \rho_{gb} \frac{\dot{M}_\delta}{\dot{M}_g} \cdot \frac{u_g}{u_\delta}.$$

Now, heat transfer between vapor and droplets suspended in the stream is considered. Heat transfer to a droplet evaporating in the superheated stream is affected by vapor efflux from the droplet surface and the heat-transfer coefficient becomes lower than that of a solid sphere [14–19]. Ross *et al.* [14, 15] have carried out experimental and theoretical investigations into this phenomenon. They have shown that the heat-transfer coefficient of an evaporating droplet, $\alpha_{g\delta*}$, can be expressed as

$$\alpha_{g\delta*} = \gamma(B)\alpha_{g\delta*0}, \tag{10}$$

where $\alpha_{g\delta*0}$ is the heat-transfer coefficient of a solid sphere in the absence of evaporation. $\gamma(B)$ represents the effect of vapor efflux and is usually referred to as a shielding function. $B = c_{pgf*}(T_g - T_s)/(h_{fg} - \dot{q}_{rad}/\dot{m})$ is the non-dimensional Spalding transport number, where c_{pgf*} is the specific heat of vapor, $\dot{q}_{rad}$ the heat flux due to radiation and $\dot{m}$ the vaporization mass flux (in the present investigation the radiation effect can be ignored). Subscripts $\delta*$ and $f*$ refer to the value per unit surface area of the droplet and the property value evaluated at the droplet film temperature $T_{f*} = (T_g + T_s)/2$, respectively. They have also suggested that the shielding function is approximated by the form

$$\gamma(B) = \ln(1+B)/B \tag{11}$$

and that the heat-transfer coefficient in the absence of evaporation is written as

$$\alpha_{g\delta*0} = \frac{\lambda_{gf*}}{\bar{d}_2} \{2 + \tfrac{9}{16} Re_\delta Pr_{gf*} + \tfrac{9}{64} (Re_\delta Pr_{gf*})^2\} \tag{12}$$

in a range of low droplet Reynolds numbers,

$$Re_\delta = (u_g - u_\delta)\bar{d}_2/v_{gf*};$$

and

$$\alpha_{g\delta*0} = \frac{\lambda_{gf*}}{\bar{d}_2} (2 + 0.355 Re_\delta^{0.59} Pr_{gf*}^{1/3}) \tag{13}$$

in a range of high Re_δ from 20 to 200. Here we adopt the results of Ross *et al.* to the present analysis. Under the experimental conditions of [1], the

droplet Reynolds number was less than 100, and Prandtl number of R-113 vapor was about 0.79. Then equation (12) is applied in a range of $Re_\delta \leqq 0.1$, and equation (13) in $Re_\delta > 10$. In the intermediate range of $0.1 < Re_\delta \leqq 10$, a log–linear interpolation of the convective term of equation (12) at $Re_\delta = 0.1$ and that of equation (13) at $Re_\delta = 10$ is introduced. The resultant relationships are

$$\frac{\alpha_{g\delta*}}{\ln(1+B)/B} = \begin{cases} \dfrac{\lambda_{gf*}}{\bar{d}_2}(2+0.444Re_\delta+0.0875Re_\delta^2), & Re_\delta \leqq 0.1 \\ \dfrac{\lambda_{gf*}}{\bar{d}_2}(2+0.26Re_\delta^{0.725}), & 0.1 < Re_\delta \leqq 10 \\ \dfrac{\lambda_{gf*}}{\bar{d}_2}(2+0.328Re_\delta^{0.59}), & Re_\delta > 10 \end{cases}. \tag{14}$$

The heat-transfer rate from vapor per unit surface area of the droplet is given by

$$\dot{q}_{g\delta*} = \alpha_{g\delta*}(T_g - T_s). \tag{15}$$

In the present cases droplet breakup in the stream may be ignored, because a droplet Weber number $We = \rho_g(u_g - u_\delta)^2\bar{d}_2/\sigma$ is estimated to be much smaller than the critical Weber number ($\doteqdot 20$), as is pointed out in the previous paper [1]. Ueda *et al.* [13] have observed that droplets impinging on a vertical hot surface bounce without breakup when $We_w = \rho_l u_{\delta w}^2 d/\sigma \leqq 70$. Transverse velocity of a droplet is induced by the turbulent fluctuation of vapor flow. Generally, velocity fluctuation of the vapor in turbulent flow through a tube is smaller than the mean flow velocity by an order of magnitude. Even if the component of droplet velocity normal to the tube wall, $u_{\delta w}$, is assumed to be one tenth of the mean vapor velocity, We_w in the present experimental conditions is estimated to range from 6 to 60. Therefore, it may be reasonable to assume that droplets do not break up by impingement on the tube wall. Thus, a conservation law holds as to the number of droplets passing through the tube at any axial position referring to that at the dryout point:

$$N \cdot u_\delta = N_{DP} \cdot u_{\delta DP}, \tag{16}$$

where N is the number density of droplets and subscript DP refers to the dryout point. N_{DP} is obtained from the liquid flowrate as

$$N_{DP} = \frac{\dot{M}_T(1-x_{EDP})}{\dfrac{\pi}{6}(\bar{d}_4)_{DP}^3 \rho_{ls} \cdot \dfrac{\pi}{4} D^2 u_{\delta DP}} = \frac{24\dot{M}_T(1-x_{EDP})}{\pi^2 D^2 (\bar{d}_4)_{DP}^3 \rho_{ls} u_{\delta DP}}, \tag{17}$$

where ρ_{ls} is the density of the saturated liquid. From the ratio of the total surface area of droplets in unit length of the tube, $\pi(\bar{d}_2)^2(\pi D^2 N/4)$, to the wall surface area of unit length of the tube, πD, $\dot{q}_{g\delta*}$ defined per unit surface area of droplets is converted to $\dot{q}_{g\delta}$ per unit surface area of the tube wall as follows:

$$\dot{q}_{g\delta} = \frac{\pi D(\bar{d}_2)^2 N}{4}\dot{q}_{g\delta*}. \tag{18}$$

Substitution of $\dot{q}_{w\delta}$ from equation (9) into equation (1) gives $\dot{q}_{wg}$, and then substituting this into equation (8) yields the wall temperature T_{wi}. Execution of the above calculation, however, necessitates the knowledge of the droplet diameter d, the actual quality x_A, the vapor temperature T_g and the droplet velocity u_δ.

3.2. *Basic equations for* d, x_A, T_g *and* u_δ

The total heat-transfer rate per unit surface area of droplets, $\dot{q}_{\delta*}$, is obtained from equations (2), (9), (15) and (18) as

$$\dot{q}_{\delta*} = \frac{4}{\pi D(\bar{d}_2)^2 N}\varepsilon\dot{m}_D h_{fg} + \alpha_{g\delta*}(T_g - T_s). \tag{19}$$

The rate of change of droplet volume by vaporization gives the following equation:

$$-\frac{\pi}{6}\rho_{ls}\frac{\mathrm{d}}{\mathrm{d}t}(\bar{d}_4)^3 = \frac{\dot{q}_{\delta*}\pi(\bar{d}_2)^2}{h_{fg}}.$$

Introducing $(\mathrm{d}/\mathrm{d}t)\bar{d}_4 = u_\delta(\mathrm{d}/\mathrm{d}z)\bar{d}_4$ yields

$$-\frac{\mathrm{d}}{\mathrm{d}z}(\bar{d}_4) = \frac{1}{u_\delta}\frac{2\dot{q}_{\delta*}}{h_{fg}\rho_{ls}}\frac{(\bar{d}_2)^2}{(\bar{d}_4)^2}. \tag{20}$$

The rate of droplet vaporization in an increment of tube length Δz is expressed as $(\pi D^2 \cdot \Delta z \cdot N/4)\pi(\bar{d}_2)^2\dot{q}_{\delta*}/h_{fg}$. This is equal to the increase in the vapor flowrate, $\dot{M}_T\Delta x_A$. Therefore,

$$\frac{\mathrm{d}x_A}{\mathrm{d}z} = \frac{\pi^2 D^2(\bar{d}_2)^2 N\dot{q}_{\delta*}}{4\dot{M}_T h_{fg}}. \tag{21}$$

The heat from the tube wall is ultimately consumed to superheat the vapor, to evaporate droplets and to superheat the evaporated vapor to the bulk temperature. Then, the heat balance requires

$$\frac{\mathrm{d}T_g}{\mathrm{d}z} = \frac{1}{x_A c_{pgb}}\left[\frac{\pi D\dot{q}_w}{\dot{M}_T} - \{h_{fg} + (T_g - T_s)c_{pgf*}\}\frac{\mathrm{d}x_A}{\mathrm{d}z}\right], \tag{22}$$

where c_{pgb} is the specific heat of vapor at the bulk temperature.

Force balance on droplets which are entrained in upward flowing vapor can be written in the form:

$$\frac{\pi}{6}(\bar{d}_4)^3\rho_{ls}\frac{du_\delta}{dt} = \tfrac{1}{2}C_D\rho_{gf*}(u_g-u_\delta)^2\frac{\pi}{4}(\bar{d}_2)^2 - \frac{\pi}{6}(\bar{d}_4)^3\rho_{ls}g - \frac{\pi}{6}(\bar{d}_4)^3\frac{dp}{dz},$$

where the first term on the RHS is the drag force due to the relative flow of vapor, and C_D is the drag coefficient. The second term denotes the gravity force and the third the force due to pressure gradient. Substituting $du_\delta/dt = u_\delta(du_\delta/dz)$, the above equation reduces to

$$\frac{du_\delta}{dz} = \frac{1}{u_\delta}\left[0.75C_D\frac{\rho_{gf*}}{\rho_{ls}}\frac{(\bar{d}_2)^2}{(\bar{d}_4)^3}\times(u_g-u_\delta)^2 - g - \frac{1}{\rho_{ls}}\frac{dp}{dz}\right]. \quad (23)$$

taneously determined from equations (1) and (8) as mentioned previously. The initial conditions of integration are as follows. Since droplets do not evaporate nor break up in the upper stream of the dryout point, as mentioned in [1], the empirical equation (6) of [1] which was reduced from the measurement of droplet sizes at the inlet of the test tube are applied to determine the initial value of $\bar{d}_4$ at the dryout point. As the vapor and liquid phases are in an equilibrium state up to the dryout point, $x_A = x_E$ and $T_g = T_s$ at the dryout point. The ratio of the velocities of vapor and droplets is assumed to be $u_g/u_\delta = 1.1$ at the dryout point [27]. In the course of calculation, however, it has been proved that whichever value between 1.0 and 1.1 we may choose for u_g/u_δ at the dryout point, the predicted value of u_g-u_δ converges to a single curve rapidly downstream from the dryout point, giving almost the same results of T_g and T_{wi}.

Table 1. Basic parameters of experimental runs

No. of Fig.	p_{in} bar	$\dot{M}_T$ kg/h	x_{in}	$\dot{q}_w$ W/m^2	x_{DP}	$\dot{M}_{gDP}$ kg/h	$\dot{M}_{\delta DP}$ kg/h
3	3.08	254	0.628	2.13×10^4	0.698	177	76.7
4	3.08	251	0.626	8.41×10^4	0.656	165	86.3
5	3.09	221	0.721	7.14×10^4	0.740	164	57.5
6	3.04	326	0.491	7.20×10^4	0.521	170	156
7	3.06	153	0.459	5.12×10^4	0.745	114	39.0
8	3.09	221	0.711	4.98×10^4	0.747	165	55.9

It has been known that the drag force acting on an evaporating droplet varies from that in the absence of evaporation. An amount of works have been done on this subject [16, 20–25]. In the present analysis we adopt the result of Eisenklam *et al.* [16]. They measured the drag forces acting on droplets which were falling in a stagnant gas at high temperatures. They suggested that C_D is expressed in terms of the drag coefficient of a solid sphere C_{DO} and the foregoing non-dimensional Spalding transport number B as follows:

$$C_D = \frac{1}{1+B}C_{DO}. \quad (24)$$

Variation of C_{DO} with Re_δ is well established and is approximated as follows [26]:

$$C_{DO} = \begin{cases} \dfrac{24}{Re_\delta} & Re_\delta \leqq 2 \\ \dfrac{18.5}{Re_\delta^{0.6}} & 2 < Re_\delta \leqq 500 \\ 0.44 & Re_\delta > 500 \end{cases}. \quad (25)$$

Equations (20)–(23) are integrated step by step by Runge–Kutta–Gill method starting from the dryout point. At the time of integration, evaluations of $\dot{q}_{w\delta}$ and $\dot{q}_{g\delta*}$ in equations (9) and (15) are involved to estimate $\dot{q}_{\delta*}$ in equation (19), and T_{wi} is simul-

4. PREDICTED RESULTS AND DISCUSSIONS

Typical results of the analysis are illustrated in Figs. 3—8. In Table 1 the basic parameters of the experimental runs are listed in the second to the fifth columns. In the sixth column is the quality at the dryout point, x_{DP}, calculated from equation (5) by substituting the value of z where the measured wall temperature began to rise sharply. In the last two columns are the mass flowrate of vapor at the dryout point, $\dot{M}_{gDP} = \dot{M}_T x_{DP}$, and that of droplets, $\dot{M}_{\delta DP} = \dot{M}_T(1-x_{DP})$. Between Figs. 3 and 4 values of $\dot{M}_{gDP}$ and $\dot{M}_{\delta DP}$ are almost equivalent but $\dot{q}_w$ is much different. Comparison between Figs. 5 and 6 is expected to make clear the effect of difference in droplet mass flow-rate at the dryout point, and so are Figs. 7 and 8 the effect of vapor mass flow-rate at the dryout point. Abscissas of Figs. 3–8 denote the equilibrium quality defined by equation (5). In the upper parts of the figures are shown computed results of $\bar{d}_1$, x_A, T_g, u_g-u_δ and T_{wi}, and in the under parts are various heat-transfer rates. Solid lines represent the results obtained by assuming the heat-transfer effectiveness of impinging droplets $\varepsilon = 0$, while broken lines assume $\varepsilon = 1$. Results assuming $\varepsilon = 0.2$ are also plotted by solid lines for T_{wi}. Circular plottings in the upper part are the inner wall temperatures calculated from the wall temperatures measured at the outer surface of the tube, and a

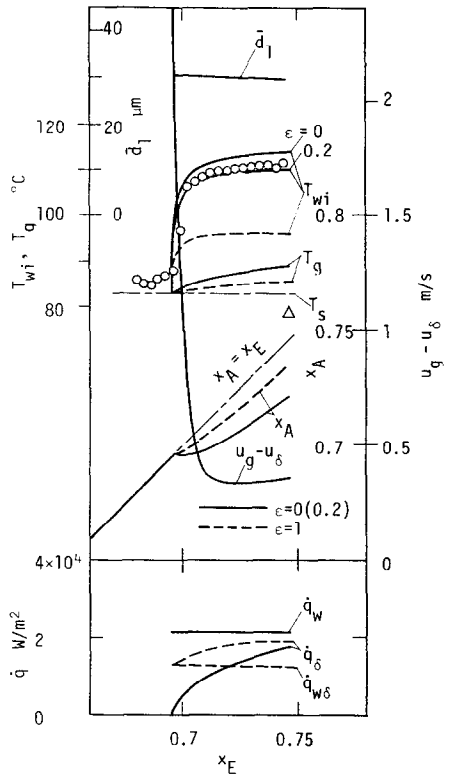

FIG. 3. Comparison between measured and predicted results (1).

triangular plot is the vapor temperature measured by the suction thermometer at the exit of the tube. In the upper parts of Figs. 6 and 8, only the values of T_{wi} are plotted.

From Figs. 3 and 4 it can be said that the measured wall superheat, $T_{wi}-T_s$, is nearly in proportion to the wall heat flux $\dot{q}_w$ under similar flowrates of vapor $\dot{M}_{gDP}$ and of droplets $\dot{M}_{\delta DP}$ at the dryout point. Further comparison between Figs. 5 and 6 along with one between Figs. 7 and 8 demonstrates that the overall heat-transfer coefficient in the post dryout region is not so much affected by $\dot{M}_{\delta DP}$ but is roughly determined by $\dot{M}_{gDP}$. An insight into the distributions of various heat fluxes shown in the under parts of Figs. 3–8 makes the underlying mechanism clearer. In the upstream part of the dryout point the rate of the liquid film evaporation by the wall heat flux, $\dot{q}_w/h_{fg}$, exceeds the rate of droplet mass transfer onto the liquid film, $\dot{m}_D$, resulting in the eventual dryout of the liquid film [1]. Then, since $\dot{m}_D$ changes gradually, the heat-transfer rate from wall to droplets, $\dot{q}_{w\delta}$, given by equation (9) in the post dryout region becomes considerably smaller than the wall heat flux $\dot{q}_w$, as is seen in Figs. 3–8, even in the case where the heat-transfer effectiveness of impinging droplets is assumed $\varepsilon = 1$. Further, comparison between the measured and calculated wall temperature distributions in these figures suggests that the actual value of ε may be in the range from 0 to 0.2. Then the actual $\dot{q}_{w\delta}$ is estimated to be far smaller than $\dot{q}_w$. This implies that the heat from the tube wall is principally transferred to the vapor flow.

Heat transfer between vapor and droplets, namely, droplet evaporation is characterized by the distributions of $\dot{q}_{g\delta} = \dot{q}_\delta - \dot{q}_{w\delta}$ ($= \dot{q}_\delta$ in the case where $\varepsilon = 0$) in Figs. 3–8. From equations (10)–(15) and (18), $\dot{q}_{g\delta}$ increases with the velocity difference

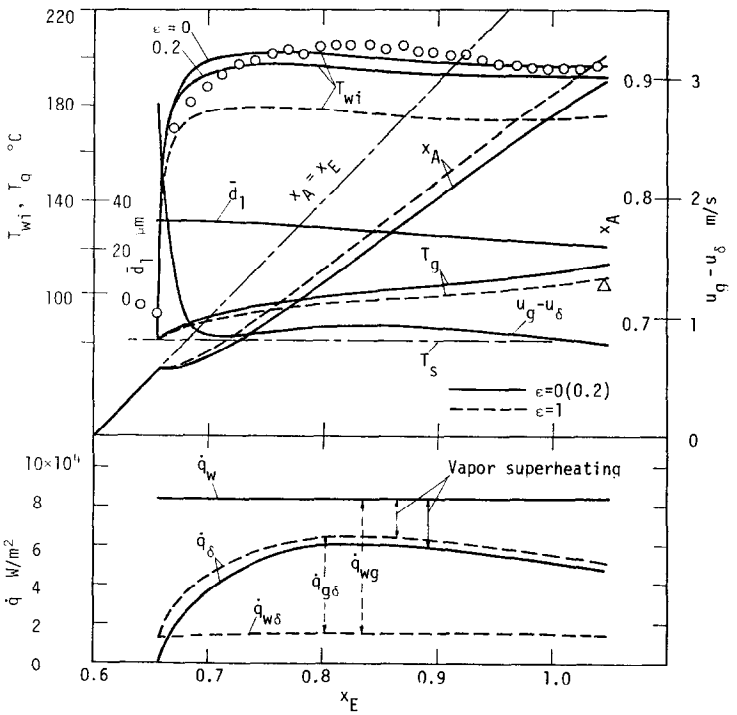

FIG. 4. Comparison between measured and predicted results (2).

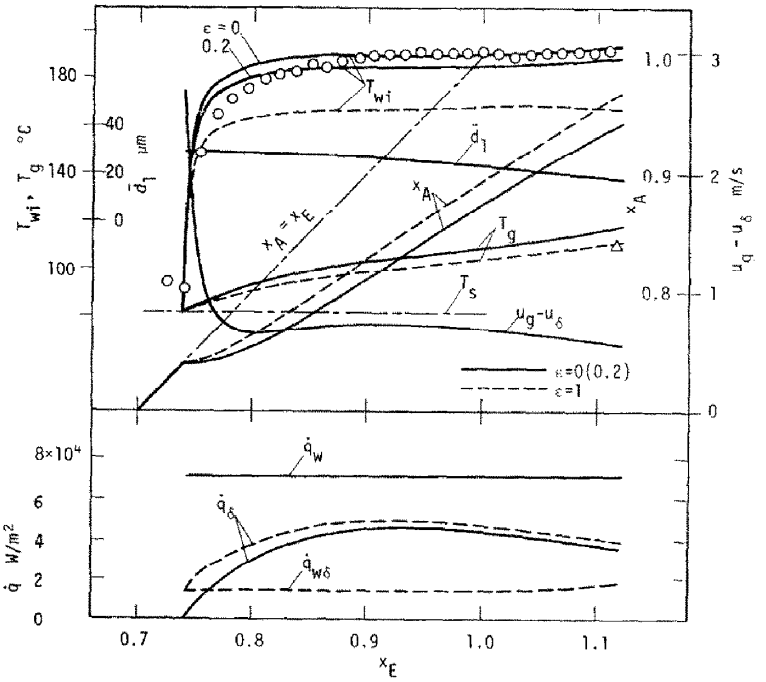

FIG. 5. Comparison between measured and predicted results (3).

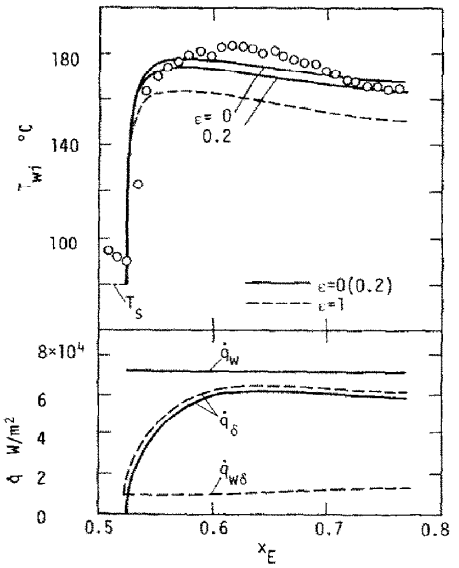

FIG. 6. Comparison between measured and predicted results (4).

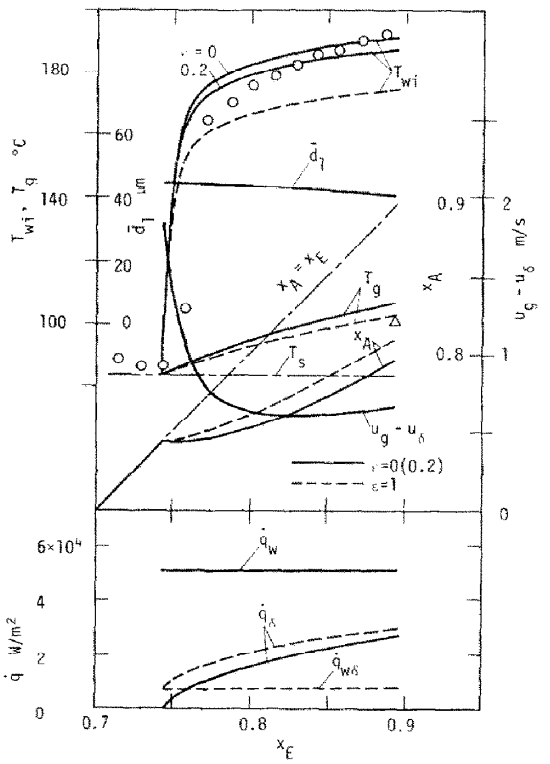

FIG. 7. Comparison between measured and predicted results (5).

between vapor and droplets, $u_g - u_\delta$, and is in proportion to the vapor superheat, $T_g - T_s$, and also to the total surface area of droplets per unit volume, $\pi \bar{d}_2^2 N$. On the other hand, the vapor superheat $T_g - T_s$ is motivated from $\dot{q}_{wg} - \dot{q}_{g\delta} = \dot{q}_w - \dot{q}_\delta$, as is explained in the under part of Fig. 4. At the dryout point, $T_g - T_s = 0$ and $\dot{q}_{g\delta} = 0$, yielding $dx_A/dz \neq 0$ from equation (21). Downstream from the dryout point $\dot{q}_{g\delta}$ first increases rapidly with $T_g - T_s$. When $\dot{M}_{\delta DP}$ (in the strict sense $\pi \bar{d}_2^2 N$) is sufficiently large as is the case in Fig. 6, $\dot{q}_{g\delta}$ increases near to $\dot{q}_w$ in a short distance downstream. The distribution of $\dot{q}_{g\delta}$ becomes almost flat in some distance downstream as the result of the compensating effects of the increase in $T_g - T_s$ and the decrease in $\pi \bar{d}_2^2 N$, leaving a considerable margin of $\dot{q}_w - \dot{q}_\delta$ for superheating the vapor. Downstream from this region, the vapor

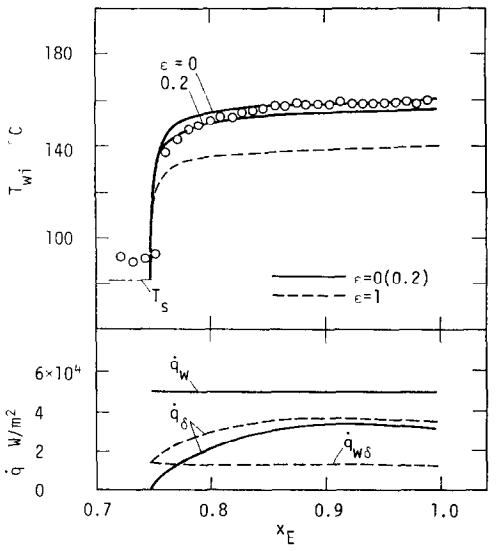

FIG. 8. Comparison between measured and predicted results (6).

superheat $T_g - T_s$ and the actual quality x_A vary roughly in a linear manner until the point near to $x_A = 1$ where liquid droplets vanish (see Figs. 4 and 5).

As for the vapor temperatures measured at the exit of the test tube, considerably superheated values were actually obtained as shown in Figs. 4, 5 and 7. Especially in the case of Fig. 7, the equilibrium quality x_E at the exit is still less than unity. The measured vapor temperatures, however, seem to be deviated to the lower side due to difficulties involved in the measurement.

5. CONCLUSION

Experimental data of heat transfer in the post dryout region of R-113 upward high quality flow in a uniformly heated tube were compared with the analytical predictions based on the three path heat-transfer model, involving heat-transfer processes from wall to vapor, from vapor to liquid droplets, and from wall to droplets in contact with the wall. From the result, it was concluded that in the post dryout region most part of heat from the tube wall is transferred to the vapor flow, while droplets impinging on the wall remove only a small part of heat. Thus the vapor, being at the saturation temperature at the dryout point, is superheated progressively as it flows downstream of the dryout point. In a fairly downstream region, the droplet vaporization in the superheated vapor stream proceeds roughly at a constant rate, and then the vapor superheat as well as the actual quality increases approximately in a linear manner.

REFERENCES

1. T. Ueda, H. Tanaka and Y. Koizumi, Dryout of liquid film in high quality R-113 upflow in a heated tube, in *Proceedings of the 6th International Heat Transfer Conference, Paper No. FB-26*, Toronto (1978).
2. H. S. Swenson, J. R. Carver and G. Szoeke, The effects of nucleate boiling versus film boiling on heat transfer in power boiler tubes, *Trans. ASME, J. Engng Pwr* **84**, 365–371 (1962).
3. E. E. Polomik, S. Levy and S. G. Sawochka, Film boiling of steam–water mixtures in annular flow at 800, 1100, 1400 psi, *J. Heat Transfer* **86**, 81–88 (1964).
4. W. F. Laverty and W. M. Rohsenow, Film boiling of saturated nitrogen flowing in a vertical tube, *J. Heat Transfer* **89**, 90–98 (1967).
5. R. P. Forslund and W. M. Rohsenow, Dispersed flow film boiling, *J. Heat Transfer* **90**, 399 407 (1968).
6. S. J. Hynek, W. M. Rohsenow and A. E. Bergles, Forced-convection, dispersed-flow film boiling, MIT Dept. of Mech. Engng Rept., No. 70586-63 (1969).
7. D. N. Plummer, O. C. Iloeje, W. M. Rohsenow, P. Griffith and E. N. Ganic, Post critical heat transfer to flowing liquid in a vertical tube, MIT Dept. of Mech. Engng Rept., No. 72718-91 (1974).
8. O. C. Iloeje, D. N. Plummer, W. M. Rohsenow and P. Griffith, A study of wall rewet and heat transfer in dispersed vertical flow, MIT Dept. of Mech. Engng Rept., No. 72718-92 (1974).
9. O. C. Iloeje, D. N. Plummer, W. M. Rohsenow and P. Griffith, An investigation of the collapse and surface rewet in film boiling in forced vertical flow, *Trans. ASME, Ser. C* **97**, 166–172 (1975).
10. A. W. Bennett, G. F. Hewitt, H. A. Kearsey and R. K. F. Keeys, Heat transfer to steam–water mixtures flowing in uniformly heated tubes in which the critical heat flux has been exceeded, *AERE-R* 5373 (1976).
11. R. K. F. Keeys, J. C. Ralph and D. N. Roberts, Post-burnout heat transfer in high pressure steam–water mixtures in a tube with cosine heat flux distribution, in *Progress in Heat and Mass Transfer*, Vol. 6, pp. 99–118 (1971).
12. C. A. Depew, Heat transfer to air in a circular tube having uniform heat flux, *J. Heat Transfer* **84**, 186–187 (1962).
13. T. Ueda, T. Enomoto and M. Kanetsuki, Heat transfer characteristics and dynamic behavior of saturated droplets impinging on a heated vertical surface, in *Proceedings of the 15th Japan National Heat Transfer Symposium*, pp. 283–285 (1978).
14. T. W. Hoffman and L. L. Ross, A theoretical investigation of the effect of mass transfer on heat transfer to an evaporating droplet, *Int. J. Heat Mass Transfer* **15**, 599–617 (1972).
15. L. L. Ross and T. W. Hoffman, Evaporation of droplets in a high temperature environment, in *Proceedings of the 3rd International Heat Transfer Conference*, Vol. 5, pp. 50–59 (1966).
16. P. Eisenklam, S. A. Arunachalam and J. A. Weston, Evaporation rates and drag resistance of burning drops, in *11th Symposium on Combustion*, 715–728 (1967).
17. S. Kotake and T. Okazaki, Evaporation and combustion of a liquid droplet, *Trans. Japan Soc. Mech. Engrs* **34**, 2191–2199 (1968).
18. K. Kobayashi, On the evaporative velocity of a liquid droplet in a high temperature gas, *Trans. Japan Soc. Mech. Engrs* **15**, 14–19 (1949).
19. J. Montlucon, Heat and mass transfer in the vicinity of an evaporating droplet, *Int. J. Multiphase Flow* **2**, 171–182 (1975).
20. N. Araki, M. Azuma, M. Nakagawa and K. Kobayashi, Drag coefficient of an evaporating droplet, in *Proceedings of the 11th Japan National Heat Transfer Symposium*, pp. 185–188 (1974).
21. N. Araki and M. Iwata, Drag coefficient of an evaporating droplet, in *Proceedings of the 12th Japan National Heat Transfer Symposium*, 593–596 (1975).
22. M. Ogasawara, T. Adachi and Y. Yashiki, Study on the drag of a cylinder and a sphere of liquid fuel with flame,

Trans. Japan Soc. Mech. Engrs **33**, 277–284 (1967).
23. T. Uematsu, T. Adachi, K. Taku and M. Tanbara, Study on the drag of a cylinder with air blowing in an air stream, *Trans. Japan Soc. Mech. Engrs* **37**, 1309–1315 (1971).
24. R. D. Ingebo, Vaporization rates and drag coefficients for isooctane sprays in turbulent air streams, *NACA TN* 3265 (1954).
25. R. D. Ingebo, Drag coefficient for droplets and solid spheres in clouds accelerating in airstream, *NACA TN* 3762 (1956).
26. R. B. Bird, W. E. Stewart and E. N. Lightfoot, *Transport Phenomena*, p. 192. John Wiley, New York (1960).
27. S. Namie and T. Ueda, Droplet transfer in two-phase annular mist flow (Part 1, Experiment of droplet transfer rate and distributions of droplet concentration and velocity), *Bull. J.S.M.E.* **15**, 1568–1580 (1972).

TRANSFERT THERMIQUE DE POST-ASSECHEMENT POUR UN ECOULEMENT ASCENDANT DE R-113 DANS UN TUBE VERTICAL

Résumé—On analyse le transfert thermique dans la région de l'assèchement pour un tube chauffé uniformément, sur la base d'un modèle à trois parcours, englobant les mécanismes de transfert thermique de la paroi vers la vapeur, de la vapeur vers les gouttes liquides, et de la paroi vers les gouttes en contact avec elle. On calcule la distribution de température pariétale en résolvant un système d'équations qui décrit les variations du diamètre de goutte, la qualité et la température de la vapeur et la vitesse de la goutte le long du tube en aval du point d'assèchement. Les distributions calculées de la température pariétale s'accordent bien avec les résultats expérimentaux présentés pour R-113 dans un article précédent. Ce résultat montre que la majeure partie de la chaleur est transférée de la paroi à l'écoulement de vapeur et que les gouttes se vaporisent principalement dans l'écoulement de vapeur surchauffée.

WÄRMEÜBERGANG AN R113 NACH DEM DRYOUT BEI AUFWÄRTSGERICHTETER STRÖMUNG IM SENKRECHTEN ROHR

Zusammenfassung—Es wurde eine Untersuchung des Wärmeüberganges im Anschluß an das Dryout-Gebiet bei aufwärtsgerichteter Srtömung in einem senkrechten Rohr auf der Grundlage des Dreiwege-Wärmeübergangsmodells durchgeführt. Dieses erfaßt die Wärme-übergangsvorgänge zwischen Wand und Dampf, zwischen Dampf und Flüssigkeitstropfen und zwischen Wand und dem die Wand berührended Tropfen. Die Temperaturverteilung in der Wand wurde durch die Lösung eines Satzes von Gleichungen berechnet, welche die Veränderung des Tropfendurchmessers, den momentanen Dampfgehalt, die Dampftemperatur und die Tropfengeschwindigkeit längs des Rohres, stromabwärts nach dem Dryout-Punkt, beschreiben. Die berechnete Temperaturverteilung in der Wand zeigt eine gute Übereinstimmung mit den experimentellen Befunden für R113, die in einem früheren Bericht veröffentlicht wurden. Das Ergebnis zeigt, daß der größte Teil der Wärme von der beheizten Wand an den Dampfstrom übertragen wird und daß die Tropfen hauptsächlich im überhitzten Dampfstrom verdampfen.

ПЕРЕНОС ТЕПЛА ЗА ОСУШЕННОЙ ОБЛАСТЬЮ ВОСХОДЯЩЕГО ПОТОКА R-113 В ВЕРТИКАЛЬНОЙ ТРУБЕ

Аннотация — На основе трёхступенчатой модели переноса тепла, включающей процессы переноса тепла от стенки к пару, от пара к каплям жидкости и от стенки к находящимся в контакте с ней каплям, проведен анализ переноса тепла за осушенной областью восходящего потока в вертикальной трубе. Распределение температуры стенки рассчитывалось путём решения системы уравнений, описывающих изменения диаметра капель, температуры пара и скорости капель вдоль трубы. Полученные распределения температуры стенки хорошо согласуются с экспериментальными данными для R-113, представленными в предыдущей работе. Этот результат свидетельствует о том, что бóльшая часть тепла от поверхности нагрева передаётся потоку пара, и капли испаряются главным образом в потоке перегретого пара.